Journal of Colloid and Interface Science 353 (2011) 290–293

Contents lists available at ScienceDirect

Journal of Colloid and Interface Science

www.elsevier.com/locate/jcis

Absorption and transport properties of ultra-fine cellulose webs

Gerardo Callegari [a,*], Ilya Tyomkin [a], Konstantin G. Kornev [b], Alexander V. Neimark [c], You-Lo Hsieh [d]

[a] TRI/Princeton, Princeton, NJ, USA
[b] School of Materials Science and Engineering, Clemson University, Clemson, SC, USA
[c] Chemical Engineering Department, Rutgers University, Piscataway, NJ, USA
[d] Fiber and Polymer Science, University of California at Davis, Davis, CA, USA

ARTICLE INFO

Article history:
Received 25 May 2010
Accepted 3 September 2010
Available online 15 September 2010

Keywords:
Permeability
Wicking
Pore size
Electrospinning
Cellulose
Nanoweb
Kozeny–Carman
Washburn

ABSTRACT

Characterization of transport and absorption properties of nanofiber webs is a challenge, because in many cases the material is soft and cannot withstand the stresses exerted by the standard instruments. In this paper, we report on development of a new technique for materials characterization. We propose to conduct wicking and permeability experiments for full characterization of the nanowebs. As an example, we used electrospun cellulose acetate nanowebs. The wicking experiments showed very good reproducibility, demonstrating the square-root-of-time dependence of wetting front position vs time. The prefactor depends on a product of capillary pressure and materials permeability. We developed a technique to independently measure the permeability of small samples of nanowebs. Wicking and permeability data allow one to estimate the pore size; SEM micrographs confirmed the obtained estimates of pore radius. In general, the proposed method allows one to characterize the transport and absorption parameters of the nanofibrous materials for which the standard procedures are inapplicable.

1. Introduction

Many materials with high specific surface area have been filled by inorganic compounds and particles in the past. The advent of electrospinning has not only enabled processing a more diverse range of polymers, some non-fiber forming by conventional methods, but also generating fibers with sub-micrometer to tens of nanometer scale diameters. These lateral dimensions of fibers are two to even three orders of magnitude smaller than those produced by conventional melt or solution spinning processes. The continuous fibrous structure is another advantage over powders or particles.

In electrospinning (ES), a polymer solution or melt droplet formed at the opening of a thin nozzle, commonly a needle, is electrically charged by high voltage to elongate into a cone which is ejected as a jet when the electrostatic force exceeds the surface tension [1–4]. This formation of water threads was discovered by George Mathias Bose in 1745 and actively used since Boys' time to spin fine fibers [5,6]. Although the process was first reported nearly three centuries ago and the first patent was filed in 1934 [7], electrospinning has only gain attention from the scientific community in the last three decades [1–4]. In recent years, the versatility of electrospinning to generate nanomaterials with unique chemical and physical properties has been reported extensively in the scientific journals as well as applied in patented technologies and even commercialized products [3,8,9]. Electrospun fibrous webs have found multiple new applications as bio-materials for tissue engineering and scaffolds [10–12], smart textiles [13–15] and many others [1–4]. In many applications, the nanofibrous webs contact with liquids. Understanding the relationships between structure and transport properties and development of the characterization methods is important for design of different structures where nanofibrous materials play a significant role [14,16,17].

Cellulose acetate (CA) nanofibers and nanowebs deserve a special attention because of their very interesting absorption properties [18]. It appears, that the water retention per fibrous mass for the electrospun CA porous membranes is nearly 10 times higher than that for fabrics of commodity fibers of similar wettability [18]. Characterization of the transport properties of these nanowebs is a challenging task because all traditional techniques deal with either nanoporous materials or materials with pore sizes larger than micrometer [19–21]. Moreover, since water–cellulose interaction produces swelling and softening of the fibers, a neutral liquid must be used to study the transport characteristics of these materials. In order to characterize the transport properties of electrospun cellulose nanowebs we bring together the methods of wicking [22–24], permeability and porosity analyses [25–28]. The proposed method gives an idea about the nano and microstructure of the fibrous material and provides a more detailed picture of the mechanism of fluid flow through nanofibrous materials. Hence, the phenomenological permeability [29] can be further studied on the basis of some microflow models. In this paper, using the wicking

* Corresponding author.
E-mail address: gcallegari@triprinceton.org (G. Callegari).

0021-9797/$ - see front matter © 2010 Elsevier Inc. All rights reserved.
doi:10.1016/j.jcis.2010.09.015

characteristics of CA nanowebs, we relate the phenomenological parameters with the structural properties of these webs. The Lucas–Washburn theory for wicking dynamics [30,31] and the Kozeny–Carman equation for permeability [32,33] are used to show the relations between the fiber size and the porosity, permeability and absorbency of the nanoweb.

2. Experimental

2.1. Cellulose nanoweb preparation and structure characterization

The cellulose fibrous web used in this study was fabricated by a previously reported method in which cellulose acetate was electrospun then fully hydrolyzed to regenerate into cellulose fibrous web [18]. Briefly, cellulose acetate (CA) (M_n = 30 kDa, 39.8 wt.% acetyl content) from Aldrich Chemical Company (Milwaukee, WI, USA) was dissolved in 2:1 w:w acetone/dimethylacetamide (DMAc). A 15 wt.% CA solution was loaded into a 20 mL glass syringe (Popper & Sons, Inc.) and delivered at 1 mL/h using a syringe pump (KDS 200, KD Scientific, USA) through a flat-end metal needle with an inner diameter of 0.31 mm. A 14.25 kV voltage by a DC power supply (ES 30-0.1 P, Gamma High Supply, USA) was applied to charge the jet to splay into finer jets to be collected onto a grounded aluminum plate placed 15 cm from the tip of the needle. The CA fibrous web was fully deacetylated into cellulose web by aqueous hydrolysis in 0.05 M NaOH at ambient temperature for 24 h, rinsed in water and vacuum dried at ambient temperature for 48 h.

The morphology of the fibrous web was observed under a scanning electron microscope (SEM) (XL 30-SFEG, FEI/Philips, USA) after sputter coated with gold (Fig. 1). The porosity ϕ of the fibrous web was measured by immersing the material in hexadecane. Hexadecane is known for its chemical inertness with respect to cellulose. It has the surface tension σ = 27 mN/m, viscosity, η = 3.34 cp, and density ρ = 773 kg/m^3. The porosity was calculated as $\phi = m_w - m_d)/(\rho V_T)$, where m_w is the mass of wet sample, m_d is the mass of dry sample, and V_T is the sample volume. We calculated the sample volume as $V_T = Ad$, where A is the sample area calculated from the sample photograph using ImageJ program, and d is the sample thickness. The sample thickness was determined by sandwiching the web between two microscope slides and measuring the gap between the plates with the 15× Lasico ocular grid mounted on the 6.3× Zeiss objective. Using this method, we obtained the thickness of our samples as d = 23 μm, and confirmed the measurements by the SEM micrographs (Fig. 1). The porosity of the nanowebs was then calculated as ϕ = 0.83.

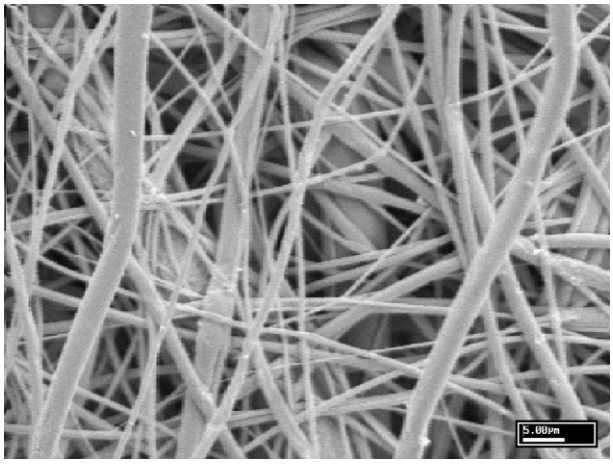

Fig. 1. Scanning Electron Microscopy top view of an electrospun cellulose nanoweb.

2.2. Wicking

In wicking tests, a strip of the electrospun material was vertically suspended and brought in contact with the hexadecane by dipping one end into the container. Filming the upward movement of the liquid through the material, one can detect the position of wetting front $L(t)$ as a function of time t. The wicking experiments were performed on four 1-cm long CA fibrous webs with the widths ranged from 5 mm to 8 mm. The illumination was provided by a backlight source. The propagation of the liquid front was captured by a digital camera (Photron Fastcam-1280) with 2-s intervals. Fig. 2a shows the typical recorded images.

ImageJ software (http://rsbweb.nih.gov/ij/index.html) was used to obtain the average position of the wetting front as a function of time. First, from each image we subtracted the reference image of the dry sample, Fig. 2b. Then the result was contrast enhanced to better define the wicking front, Fig. 2c. For further image analysis, the dry area was colored in white and the wet area was colored in black, Fig. 2d. The position of the liquid front $L(t)$ was thus well defined and measured relative to the surface of the liquid in the reservoir. In Fig. 3 we plot the square of the average position of the wetting front as a function of time.

2.3. Permeability

Experimental setup is shown in Fig. 4. A 3.3 cm wide (W) and 1.9 cm long strip of CA nanoweb with d = 23 μm thickness was placed in a gap between two highly permeable paper towels. The ends of the nanoweb were firmly attached to the nonwoven materials by gently pressing two Π-like holders together. The length of the nanoweb bridging two nonwoven materials was ℓ = 0.64 cm. Each strip of highly permeable nonwoven materials was put in contact with a reservoir. The sample was placed above the reservoirs as shown in Fig. 4. The left strip was hanging 12 cm above the left container, and the right strip was hanging 7 cm above the right container sitting on the balance dish. At these chosen heights, the electrospun material was fully saturated with the liquid. Like in siphons, the hydraulic head (which was H = 5 cm here) pushed hexadecane to flow through the nanoweb from one container to the other. Using the analytical balance (Mettler AE 160), we monitored the loss of liquid. After 2 h of flow stabilization,

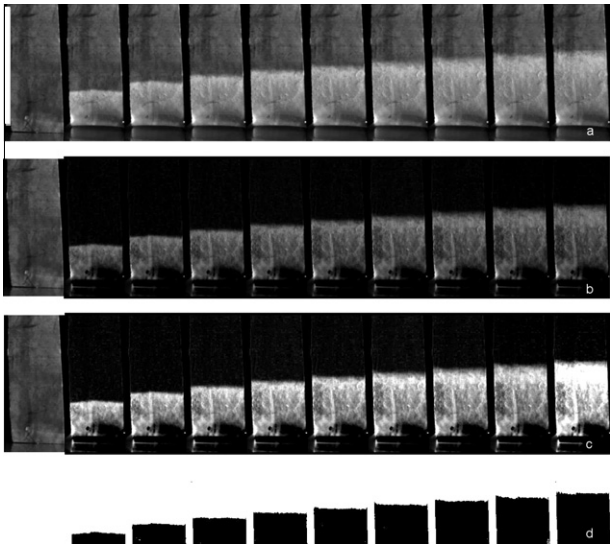

Fig. 2. Sequence of pictures showing the wetting front of hexadecane propagating through the nanoweb in the vertical direction. The time interval between frames is 2 s. The white bar is 1 cm. (a) Untreated pictures, (b) background subtraction process, (c) contrast enhancement (d) color separation of dry and wet regions.

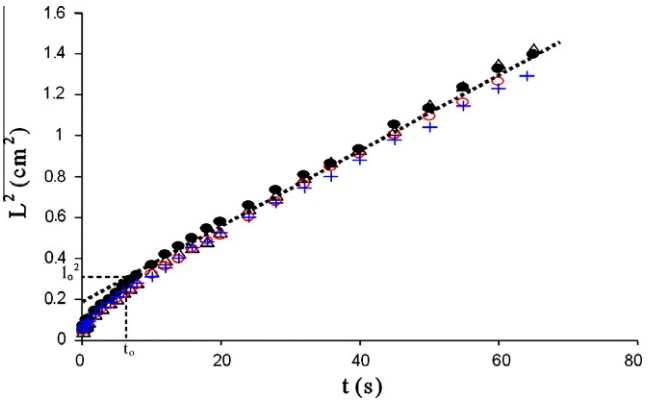

Fig. 3. The square of the position of the wetting front as a function of time. Different symbols correspond to four different experiments. The trend line corresponds to the Lucas–Washburn prediction [30,31], and it can be used for the description of the wicking kinetics at times $t > t_o$.

we measured the mass loss during 5 h. The resulting mass flux was: $Q = 1.2$ μg/s. To find the permeability k, we write Darcy's equation as $Q = dW(k/\eta)\ (\rho^2 gH)/\ell$. Substituting the experimental data, we obtain the permeability as $k = 1.1 \times 10^{-13}$ m^2.

3. Discussion

The data interpretation on wicking experiment is based on the Lucas–Washburn equation [30,31] which was modified to the flow through porous media. Using the Darcy's law and assuming that the pressure at the wetting front is constant and equal to the capillary pressure P_c, the equation for upward wicking is written as:

$$\phi \frac{dL}{dt} = \frac{k}{\eta L}(P_c - \rho g L) \tag{1}$$

where L is the position of the wicking front at time moment t. Eq. (1) describes the wicking dynamics when only viscous resistance is important. This particular regime, the Lucas–Washburn regime [30,31] is reached after time t_o corresponding to the front position $L(t_o) = l_0$. Therefore, this time moment can be set as the initial condition for Eq. (1).

In the upward wicking, the capillary pressure, which drives the process, is opposed by the hydrostatic pressure ρgL. At the moment when the hydrostatic pressure reaches the capillary pressure $L_c = P_c/\rho g$ the front stops and wicking ceases. According to the capillary model of the porous medium. i.e. considering it as a bundle of capillaries, we can call this height L_c the Jurin's height.

In the analysis of the wicking experiments based on Eq. (1), one needs to know porosity, and one of the physical parameters of the material, either capillary pressure P_c or permeability k [26].

For nanofibrous materials, the characteristic pore sizes are expected to be in the micron or even sub-micron range. Therefore, it is not practical to measure the capillary pressure through the Jurin's height, which is expected to be in the range of meters. Eq. (1) suggests that in the nanofibrous materials where the Jurin height is much greater than the sample size, the gravitational effects can be neglected. Then the solution of Eq. (1) is simplified to:

$$L^2 - l_0^2 = \alpha^2(t - t_o) \quad \text{with } \alpha = \sqrt{\frac{2P_c k}{\eta\phi}} \tag{2}$$

The parameter α in Eq. (2) can be used for the estimation of the capillary pressure. From the image analysis we found $\alpha = (0.138 \pm 0.003)$ cm/s$^{1/2}$. Substituting the permeability data, $k = 1.1 \times 10^{-13}$ m^2, we estimate the capillary pressure as $P_c \sim 24$ kPa.

Once P_c and k are obtained, it is of great interest to relate them to the structural properties of the nanofibrous material. Modeling the fibrous sample as a system of capillaries, the capillary pressure can be related to the characteristic capillary radius R_C through the Laplace law of capillarity:

$$P_c = 2\sigma/R_C \tag{3}$$

where σ is the surface tension of the liquid. This formula gives us an estimate of the pore radius responsible for building the driving capillary pressure, $R_C \sim 2.2$ μm. Because the pore radius appears to be large compared to the fiber size, this estimate suggests that the nanofiber crossings did not contribute to the driving capillary pressure at the observed time scale.

The permeability k is much more difficult to relate to the pore structure of the fibrous materials [26,33–37]. The most used expression to relate permeability with the structural parameters of fibrous materials is the Kozeny–Carman equation [32] modified for fibrous materials [33]. That is the fibrous sample is modeled as a system of capillaries with radius R_H. We distinguish R_H from R_C, because the system of transport capillaries can be different from that responsible for the capillary pressure. In this model, the permeability of the porous material can be written using the analogy with the Hagen–Poiseuille equation as $k = R_H^2/A$, where A is a constant to be determined (A is eight for a single capillary) [32]. Using a system of randomly packed 150 μm diameter rigid fibers, the authors of Ref. [33] showed that in the porosity range $0.75 < \phi < 0.85$, the materials permeability can be approximated by the formula

$$k = (\phi/4k_o)R_H^2 \tag{4}$$

with the Kozeny–Carman factor $k_o = 5.3$. Substituting the experimental value $k = 1.1 \times 10^{-13}$ m^2, we find $R_H \sim 1.7$ μm which is close to R_C defined by Eq. (3). This allows us to assume that the systems of

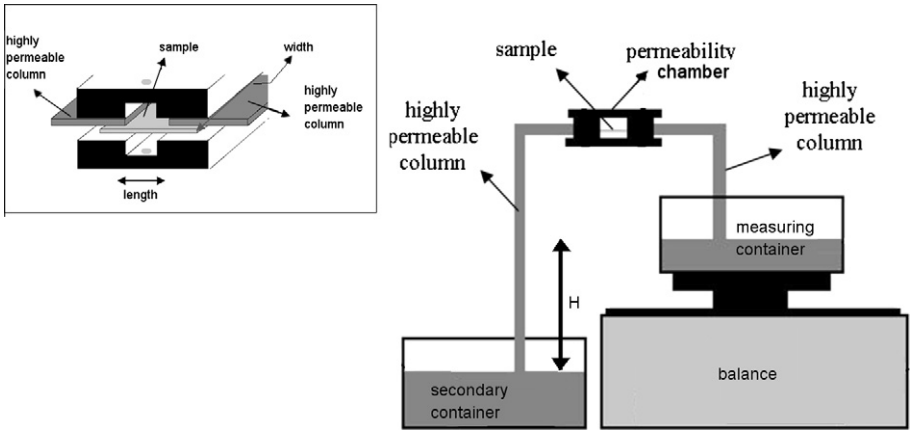

Fig. 4. Permeability apparatus. The incept in the right upper corner show details of the sample's chamber.

transport and capillary pressure pores are the same, $R_C = R_H = R$. For this model, the α-constant is rewritten as $\alpha = \sqrt{\frac{\sigma R}{\eta k_o}}$ and gives $R = 1.2$ μm. For this pore radius, the Jurin height L_c would be equal to 7 m, which is much greater than the sample height.

4. Conclusions

The cellulose acetate nanowebs were prepared by electrospinning. We conducted wicking and permeability experiments to characterize the transport and absorption properties of these materials. The wicking experiments showed very good reproducibility, indicating that the materials were homogenous on centimeter scale. The sharp wetting fronts were stable and almost straight suggesting that the nanowebs were homogenous at hundred microns/millimeter scale. The front advances following the square-root-of-time kinetics, the Lucas–Washburn kinetics. Microflow Kozeny–Carman model treating the nanofiber web as a system of capillaries proved to be sufficient to describe the experimental results. The model showed that the transport pores and the pores responsible for building the driving capillary pressure, had the same size in CA nanowebs.

In general, the proposed method allows one to characterize the transport and absorption parameters of the nanofibrous materials for which the standard procedures are inapplicable. The proposed model suggests to separate the transport pores facilitating the liquid flow, from capillary pores building up the suction pressure.

Acknowledgments

K.G.K. is supported by the NSF (Grants CMMI 0826067 and EFRI 0937985) and the Department of Commerce through the National Textile Center (Grant M10-CL03). The work was also supported by the National Textile Center (Grant M04-CD01).

References

[1] D.H. Reneker, A.L. Yarin, Polymer 49 (2008) 2387.
[2] G.C. Rutledge, S.V. Fridrikh, Adv. Drug Deliv. Rev. 59 (2007) 1384.
[3] Y. Filatov, A. Budyka, V. Kirichenko, Electrospinning of Micro- and Nanofibers: Fundamentals in Separation and Filtration Processes, Begell House Inc., Redding, CT, 2007.
[4] Y. Dzenis, Science 319 (2008) 419.
[5] C.V. Boys, Proc. Phys. Soc. London 9 (1887–1888) 8.
[6] C.V. Boys, Proc. Phys. Soc. London 13 (1894–1895) 68.
[7] A. Formhals, USA, 1934.
[8] Z.M. Huang, Y.Z. Zhang, M. Kotaki, S. Ramakrishna, Compos. Sci. Technol. 63 (2003) 2223.
[9] D. Lukas, A. Sarkar, P. Pokorny, J. Appl. Phys. 103 (2008) 084309.
[10] D.S. Katti, K.W. Robinson, F.K. Ko, C.T. Laurencin, J. Biomed. Mater. Res. Part B – Appl. Biomater. 70B (2004) 286.
[11] J. Du, Y.L. Hsieh, Cellulose 16 (2009) 247.
[12] J. Du, Y.L. Hsieh, Nanotechnology 19 (2008).
[13] H. Schreuder-Gibson, P. Gibson, K. Senecal, M. Sennett, J. Walker, W. Yeomans, D. Ziegler, P.P. Tsai, J. Adv. Mater. 34 (2002) 44.
[14] H.L. Schreuder-Gibson, M.L. Realff, MRS Bull. 28 (2003) 558.
[15] V. Reukov, A. Vertegel, O. Burtovyy, K.G. Kornevm, I. Luzinov, Mater. Sci. Eng. C 29 (2009) 669.
[16] H.L. Schreuder-Gibson, K. Senecal, M. Sennett, L. Samuelson, Z. Huang, J.-G. Wen, W. Li, Y. Ti, D. Wang, S. Yang, Z. Ren, C. Sung, Fullerenes 2000 10 (2000) 210.
[17] H.L. Schreuder-Gibson, Q. Truong, J.E. Walker, J.R. Owens, J.D. Wander, W.E. Jones, MRS Bull. 28 (2003) 574.
[18] H. Liu, Y.-L. Hsieh, J. Polym Sci., Polym. Phys. 40 (2002) 2119.
[19] F.A.L. Dullien, Powder Technol. 29 (1981) 109.
[20] A.E. Scheidegger, The Physics of Flow through Porous Media, University of Toronto, Toronto, 1974.
[21] F. Rouquerol, J. Rouquerol, K. Sing, Adsorption by Powders and Porous Solids, Academic Press, New York, 1999.
[22] P.K. Chatterjee, B.S. Gupta, Textile Science and Technology, vol. 13, Elsevier, New York, 2002.
[23] A.V. Neimark, S. Ruetsch, K.G. Kornev, P.I. Ravikovitch, P. Poulin, S. Badaire, M. Maugey, Nano Lett. 3 (2003) 419.
[24] N.R. Raravikar, L.S. Schadler, A. Vijayaraghavan, Y.P. Zhao, B.Q. Wei, P.M. Ajayan, Chem. Mater. 17 (2005) 974.
[25] E. Kissa, J. Colloid Interface Sci. 83 (1981) 265.
[26] E. Kissa, Text. Res. J. 66 (1996) 660.
[27] Y.L. Hsieh, Text. Res. J. 65 (1995) 299.
[28] B. Miller, I. Tyomkin, J. Colloid Interface Sci. 162 (1994) 163.
[29] P.W. Gibson, H.L. Schreuder-Gibson, D. Rivin, AIChE J. 45 (1999) 190.
[30] R. Lucas, Kolloid Z. 23 (1918) 15.
[31] E.W. Washburn, Phys. Rev. 17 (1921) 273.
[32] P.C. Carman, Flow of Gases through Porous Media, Butterworths Scientific Publications, London, 1956.
[33] O. Rahli, L. Tadrist, M. Miscevic, R. Santini, J. Fluids Eng. – Trans. ASME 119 (1997) 188.
[34] C.J. Nederveen, Tappi J. 77 (1994) 174.
[35] S. Abrate, Appl. Mech. Rev. 55 (2002) 579.
[36] M. Alava, K. Niskanen, Rep. Prog. Phys. 69 (2006) 669.
[37] G. Morren, M. Bottiglieri, S. Bossuyt, H. Sol, D. Lecompte, B. Verleye, S.V. Lomov, Compos. Part A – Appl. Sci. Manuf. 40 (2009) 244.